JCIM JOURNAL OF CHEMICAL INFORMATION AND MODELING

pubs.acs.org/jcim Article

Elucidating Enzymatic Catalysis Using Fast Quantum Chemical Descriptors

Igor Barden Grillo, Gabriel A. Urquiza-Carvalho, José Fernando Ruggiero Bachega, and Gerd Bruno Rocha*

Cite This: J. Chem. Inf. Model. 2020, 60, 578−591 Read Online

ACCESS | Metrics & More | Article Recommendations | Supporting Information

ABSTRACT: In general, computational simulations of enzymatic catalysis processes are thermodynamic and structural surveys to complement experimental studies, requiring high level computational methods to match accurate energy values. In the present work, we propose the usage of reactivity descriptors, theoretical quantities calculated from the electronic structure, to characterize enzymatic catalysis outlining its reaction profile using low-level computational methods, such as semiempirical Hamiltonians. We simulate three enzymatic reactions paths, one containing two reaction coordinates and without prior computational study performed, and calculate the reactivity descriptors for all obtained structures. We observed that the active site local hardness does not change substantially, even more so for the amino-acid residues that are said to stabilize the reaction structures. This corroborates with the theory that activation energy lowering is caused by the electrostatic environment of the active sites. Also, for the quantities describing the atom electrophilicity and nucleophilicity, we observed abrupt changes along the reaction coordinates, which also shows the enzyme participation as a reactant in the catalyzed reaction. We expect that such electronic structure analysis allows the expedient proposition and/or prediction of new mechanisms, providing chemical characterization of the enzyme active sites, thus hastening the process of transforming the resolved protein three-dimensional structures in catalytic information.

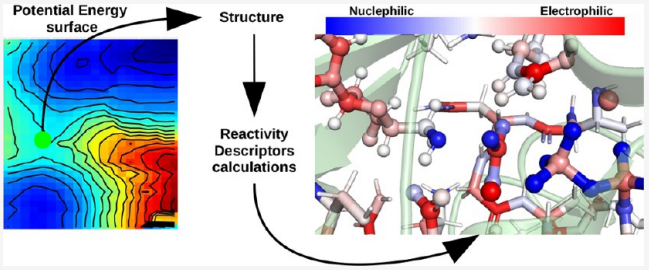

INTRODUCTION

Enzymatic catalysis allows the chemistry of life to take place in a reasonable time scale.[1] Once a genome is sequenced, millions of new protein are discovered, a small part has its three-dimensional structure determined, and even fewer have their function studied in detail. A fraction of these becomes the subject of studies about enzymatic catalysis, which is central to guide mutation studies, drug design, and technological applications for other substrates.[2]

The experimental approach is very limited to provide a desired description of these processes, mainly due to the short-lived reaction intermediates, the number of amino-acid residues, and the specifics of how their roles in the mechanism govern the catalysis.[3] Thus, the emergence of computational modeling, especially of quantum chemistry/molecular mechanics (QC/MM) hybrid methods,[4,5] has been successfully applied for reaction path determination, transition state structure optimization, and thermodynamic/kinetic properties prediction.[6]

By employing quantum chemical calculations, the theoretical characterization of the active site becomes possible with the exploration of its electronic structure.[7] Some tools for carrying out such exploration are reactivity descriptors (RDs), which are theoretical quantities that outline the propensity of a molecule/atoms to react.[8] An emblematic example of the use of such RDs in enzymatic reaction studies was their utilization for determining the most reactive angle of attack and ionization state of the phosphoenolpyruvate substrate at the 5-enolpyruvylshikimate 3-phosphate synthase active site.[9] Additionally, it is possible to find applications for the determination of the protonation states of catalytic amino-acid residues[10] and the oxidation state of arsenate ions.[11]

The RDs cited above are within the conceptual density functional theory (CDFT) framework.[8] This framework provides rigorous mathematical definitions for concepts like molecular hardness and electrophilic attack susceptibility, within the fundamental equations of the density functional theory,[12] thus bringing together reactivity theories such as the frontier molecular orbital[13] and the hard and soft acid Base theory.[14]

The application of these quantities is very extensive for small molecules,[15] being successfully employed to provide explanations in terms of generic Lewis acid/base for the majority of organic reactions, such as substitutions, eliminations, and

Special Issue: Molecular Simulation in Latin America: Coming of Age

Received: September 27, 2019
Published: January 2, 2020

https://dx.doi.org/10.1021/acs.jcim.9b00860
J. Chem. Inf. Model. 2020, 60, 578−591

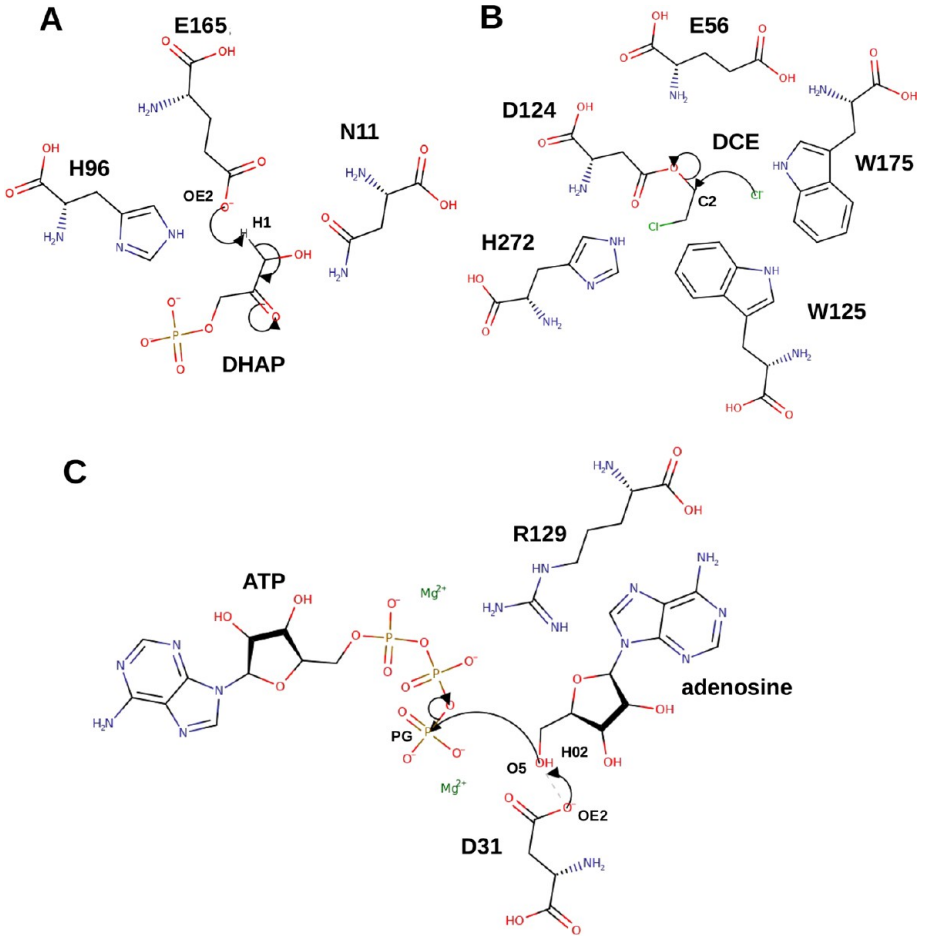

Figure 1. Reaction coordinates simulated for the first step enzymatic catalytic cycles studied in the present work: A) proton extraction by GLU165 from glycerone phosphate catalyzed by triosephosphate isomerase, B) dichloroethane formation catalyzed by haloalkane dehalogenase, and C) phosphoryl transfer from ATP to adenosine catalyzed by adenosine kinase.

additions.[16] They can be applied as global properties, representing electron transfer and polarization information,[17] and local functions as well, retrieving the bond formation and rupture propensity.[12]

In a review paper,[18] Roos and co-workers reported CDFT applications for enzymatic catalysis. According to the authors, there was resistance to fully integrate this framework with the enzymology field. Ten years afterward, this research field remains incipient. The reasons behind this may be the lack of a systematic study showing a broad application and a software to deal with the substantial information management challenges related to the electronic structure of these systems, which typically contains a large number of atoms. Also, some issues arise in the calculation of these properties for large systems, such as the lack of protocol to determine the charge disturbance for finite differences approximation[19] and the high energy degeneracy in the frontier molecular orbitals,[20] which affects the Frozen Orbital approximation.

Fukushima and co-workers[20] already showed that the specificity of enzymes is related to the localization of their frontier molecular orbitals (those with energy close to the HOMO−LUMO gap). Also, this type of information can be retrieved with semiempirical methods for the entire protein and is much less time-consuming than the QC/MM protocols using DFT functionals within a very limited QC area.

In this present work, we propose the application of CDFT RDs for monitoring the enzymatic catalysis path along the interactions between atom pairs that will form new bonds, to fully characterize the active site based on these chemical concepts.

We have used three enzymatic reaction simulations in this study. Among them we have an enzyme for which the catalysis mechanism has yet to be studied in light of theoretical quantum chemistry methods. Thus, the main goal is to test whether these RDs are capable of showing the most important energetic fluctuations using electronic structure information obtained from low level quantum chemistry computational methods.

METHODS

We used the structure files of three different enzymes to test the application of RDs along the first step in their catalytic cycle, already studied in the literature: haloalkane dehalogenase (HDH),[21] a hydrolase; triosephosphate isomerase (TIM),[22] an isomerase; and adenosine kinase (AK),[23] which is a transferase.

The reaction coordinates for these steps were generated through QC/MM relaxed scans to simulate the atom transfers taking place in the active sites of these three enzymes, depicted in Figure 1. The SCF converged electronic structure obtained from the geometry of each scan frame was used to calculate the RDs, in order to verify whether these quantities could provide

https://dx.doi.org/10.1021/acs.jcim.9b00860
J. Chem. Inf. Model. 2020, 60, 578−591

reasonable reaction profiles. Also, we have analyzed the values of these RDs for each atom in the active sites considering the key structures of these simulated reactions, which are the first geometry of the reaction coordinate, the transition state (TS), estimated here only by the heat of formation variation, and the last geometry.

QC/MM Simulations. The crystal structure files of the three enzymes were retrieved from the Protein Data Bank.[24] The substrate molecules already present in the respective active sites were parametrized with Antechamber using the GAFF force field and AM1-bcc charges[25] (AMBER18). The hydrogen atoms were added in tleap within the residue templates using the FF14SB force field, as the solvated box and neutralizing ions. The following steps were performed using pDynamo 1.9.0[26] and its interface EasyHybrid[27] to set up these calculations: (i) molecular mechanics minimization, (ii) QC/MM geometry optimization, and (iii) QC/MM relaxed scans of the reaction coordinates.

For the QC/MM geometry optimization and QC/MM reaction coordinate scans, the system was divided into the following subsystems: a QC subsystem that consists of atoms within 7.0 Å from the ones that will be transferred, in order to account for the electronic structure of all substrates and important amino-acid residues for the three enzymes; a MM subsystem within 20.0 Å from the substrate's reactive atoms that are not part of the QC subsystem; and beyond this radius up to 25.0 Å the atoms which only polarize the other two subsystems, not considering their coordinates as degrees of freedom in the geometry optimizations. This last atom group consists mainly of water molecules and very external parts of the protein. In order for this division scheme to become more clear, we depict it in Figure 2.

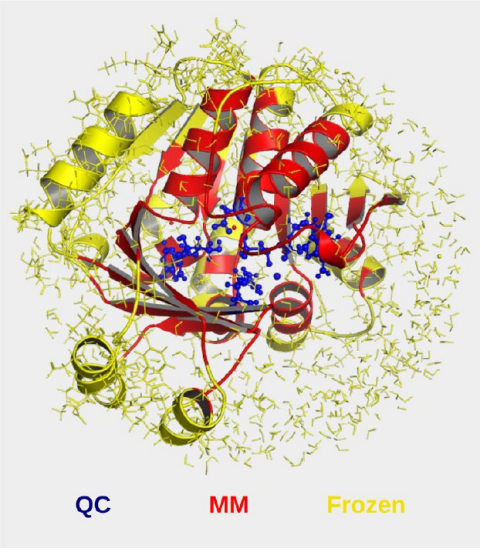

Figure 2. Division of the subsystems by the level of theory and limitations considered for the QC/MM calculations.

We applied semiempirical Hamiltonians AM1,[28] RM1,[29] PM3,[30] PM6,[31] and PM7[32] for the QC regions of all enzymes except AK, which contains Mg^{2+} cations, that do not have parameters in the RM1 Hamiltonian.

No molecular dynamics production step was performed. We understand that the chosen crystal structures already provided a satisfactory starting point for the reaction coordinate simulations, capable of generating the structures required for the hypothesis test related to the RDs performance. This was checked when our results were compared to the other works in the literature.

We have the extraction of hydrogen (H1) of dihydroxyacetone phosphate (DHAP) by the carbonyl oxygen (OE2) of GLU165, giving the enolate phosphate intermediate,[22] which constitutes the first step in the catalytic cycle of TIM, depicted in Figure 1a. The distance between H1 and OE2 in the TS geometry was set as the origin of this reaction coordinate. TIM is one of the best characterized enzymes, central to the glycolytic pathway, catalyzing the interconversion of DHAP to glyceraldehyde phosphate (GAP).[33] The active site amino-acid residues are also represented in Figure 1a: GLU165, which extracts the proton from DHAP, and HIS96, that is said to increase the acidity of the H1 and also donate a proton in one of the following catalytic steps, as well as ASN11, an important electrostatic stabilizer.[34] In the crystal structure files used for TIM (PDB: 7TIM), its inhibitor, phosphoglycolohydroxamic acid, was present in the active site, which is very similar to the DHAP. The inhibitor was further edited using the builder tool of Pymol 2.1 software to become DHAP, replacing the different atoms and adjusting the protonation, before the simulations already described in this section.

HDH is an important enzyme in biocatalysis studies for industrial applications, catalyzing the hydrolyzation of terminally chlorinated and brominated alkanes with up to four and ten carbons of chain length, respectively, producing primary alcohols.[21] We used the crystal structure 2DHC for the simulation of the first catalytic step of HDH, which is the dissociation of chlorine from the dichloroethane substrate bonded with the C2 carbon atom (Figure 1b). The reaction coordinate considered initiates with the ASP124 residue bound to the substrate and the chlorine dissociated until the formation of DCE and the detachment of ASP124 from the substrate. Within the active site, other residues are also depicted in Figure 1b, for instance TRP125 and TRP175, which are said to stabilize the chlorine ion, as well as GLU56 and HIS272, which control the reactivity of ASP124 by protonation and deprotonation.

AK is an important regulatory enzyme of purine metabolism, central to the parasitic protozoan *Toxoplasma gondii*[23] and recurring target in studies to search for inhibitors.[35] In this work, we used the crystal structure from *Mus musculus* (PDB: 5KB5), which holds 90% sequence identity with the human AK and already contains the correct substrate and ions. The reaction step simulated here combines the displacement of the P5 gamma phosphoryl group from ATP toward the O5 adenosine's ribose oxygen and the removal of a proton H02, by ASP31 residue alpha carbonyl oxygen OE2 (Figure 1c). This proton transfer to ASP31 is said to facilitate the phosphoryl transfer, but the mechanism is not certain to be either stepwise or concerted.[36] Thus, in the present study, we simulated relaxed scans simultaneously for two reaction coordinates, something we did not find in any computational QM/MM study for this enzyme. Within the described active site of AK in Figure 1c are also the ARG129 and Mg^{2+} cations, that are said to stabilize the negative charge of the transferred phosphoryl group.[36]

Table 1 summarizes information about the enzymes and data related to the QC subsystem. Among this information are the following: enzyme common name; Protein Data Bank code

https://dx.doi.org/10.1021/acs.jcim.9b00860
J. Chem. Inf. Model. 2020, 60, 578−591

Table 1. Enzyme Structures and QC/MM Enzymatic Systems Information

name	PDB (res Å)	EC	charge	QC atoms	n. frames
triosephosphate isomerase	7TIM(1.9)	5.3.1.1	−3	456	20
haloalkane dehalogenase	2DHC(2.3)	3.8.1.5	0	469	25
adenosine kinase	5KB5(1.8)	2.7.1.20	−1	482	620

of the crystal structure and the resolution of X-ray diffraction experiment; enzymatic catalysis code; formal charge of the QC subsystem; number of atoms considered by the QC Hamiltonians; and the number of scan frames carried out in the reaction coordinate simulation.

Reactivity Descriptors. In this section, we present definitions for the RDs and their conceptual explanations. The electronic chemical potential (ECP) indicates the tendency of the system to donate electrons. It is defined as the first derivative of the electronic energy with respect to the number of electrons for a constant external potential (eq 1). Hardness is defined as the second derivative of electronic energy with respect to the number of electrons for a constant external potential, and softness S is defined as its reciprocal (eq 2).[37]

$$\mu = \left(\frac{\partial E}{\partial N}\right)_{\nu} \tag{1}$$

$$\eta = 1/S = \left(\frac{\partial^2 E}{\partial N^2}\right)_{\nu} \tag{2}$$

To understand the regioselectivity of chemical reactions we use the Fukui function, which is defined as the derivative of the electron density with respect to the number of electrons (eq 3). This RD value reaches its maximum at regions where the electronic density tends to concentrate as an external nucleophilic, electrophilic, or radical influence approaching the system. This can be used to indicate where and with which orientation each type of reaction will probably take place.[38]

$$f(r) = \left(\frac{\partial \rho(r)}{\partial N}\right)_{\nu} \tag{3}$$

This descriptor was further divided into two others: the left Fukui function and the right Fukui function. The left Fukui function (f^-) is specific for electrophilic attack susceptibility (EAS), and for the frozen orbital approximation, it is equal to the HOMO density.[39] The right Fukui function (f^+) is specific for the nucleophilic attack susceptibility (NAS) and, also for the Frozen Orbital approximation, is equal to the LUMO density.

A convenient representation of the Fukui functions is one in which the values are assigned for each k-th atom center in the molecule. The f^- defined in eq 4 is the sum of each squared ν-th atomic orbital coefficient (AO) that composes the HOMO and belongs to the k-th atom plus the sum of the product between the coefficients of indices ν, μ and correspondent overlap matrix element $S_{\mu\nu}$.[40] An equivalent definition for the f^+ is presented in eq 5, using the LUMO instead of the HOMO.

$$\mathrm{EAS} = f_k^- = \sum_{\nu \in k}^{\mathrm{AO}} |C_{\nu \mathrm{HOMO}}|^2 + \sum_{\mu \neq \nu}^{\mathrm{AO}} |C_{\nu \mathrm{HOMO}} \cdot C_{\mu \mathrm{HOMO}}| S_{\mu\nu} \tag{4}$$

$$\mathrm{NAS} = f_k^+ = \sum_{\nu \in k}^{\mathrm{AO}} |C_{\nu \mathrm{LUMO}}|^2 + \sum_{\mu \neq \nu}^{\mathrm{AO}} |C_{\nu \mathrm{LUMO}} \cdot C_{\mu \mathrm{LUMO}}| S_{\mu\nu} \tag{5}$$

The electronic structure of proteins presents several relevant molecular orbitals for chemical interactions with electronic energy near the HOMO−LUMO frontier. Thus, in this study, we computed the Fukui functions using not only the HOMO and LUMO orbitals but also considering all of the molecular orbitals with energies in the range of 3.0 eV from the frontier gap. As Fukushima and co-workers showed in their work, this value can vary from 1.0 to 5.0 eV depending on the system under study.[20]

Local Hardness. The hard−hard interactions are crucial to describe a wide range of enzymatic catalysis processes, such as the transfer of groups with high charge density, e.g, proton, hydride, and phosphate ions. These reactions appear in a majority of mechanisms reported in databases.[41] There is also the soft−soft interactions, that are governed by charge transfer/electron density delocalization, that could be used to characterize covalent bonding and nucleophilic substitutions. Furthermore, the main roles the active site plays in the mechanisms are derived from its electrostatic environment.[42] Thus, special care must be taken when retrieving such information from electronic structure data.

The CDFT RD local hardness is our choice of descriptor to estimate the charge-controlled interactions in the active sites and to find key structures along reaction coordinates. Due to some ambiguity in its mathematical definition, local hardness possesses several working equations[43] which can be reliably used to compute it, and because of this we have chosen four methods to compute this RD that is found in the literature.

The definition for the first method (A) is based on the electron−electron contribution of the molecular electrostatic potential, as shown in eq 6.[44] The calculation of local hardness at the k-th atomic center is defined as a sum of the electron density for each l-th atomic center divided by their Euclidean distance R_{kl}, normalized for its N electrons. In the second method (B), eq 7, the electron density in eq 6 is approximated using the left Fukui function, which is justified by the fact that it contains the electron density most prone to interact.[45] The definition of method B is also known as the Fukui potential,[45] being equivalent to the hardness as $r \to 0$, i.e., in the atomic nucleus, representing the reactivity change with the variation of external potential.

$$H_K^{\mathrm{A}} = \frac{1}{2N} \sum_{l \neq k}^{\mathrm{atoms}} \frac{\rho(k)}{R_{kl}} \tag{6}$$

$$H_K^{\mathrm{B}} = \sum_{l \neq k}^{\mathrm{atoms}} \frac{f^-(l)}{R_{kl}} \tag{7}$$

The main source of ambiguity in the DFT definition of local hardness is the lack of a local equivalent of the electronic chemical potential to fill a similar role to that of the electron density in the local softness. To solve this, Gal and co-workers[46] proposed a working function for the local chemical

https://dx.doi.org/10.1021/acs.jcim.9b00860
J. Chem. Inf. Model. 2020, 60, 578−591

potential, providing a definition of local hardness as in eq 8 for our third method tested in this study.

$$H_K^C = \left(\rho(\mathrm{HOMO}) - \frac{\rho(k)}{N}\right)\frac{\mu}{2N} + \frac{\rho(k)}{N}\eta \tag{8}$$

The fourth method of local hardness is based on the global hardness, which is defined in terms of the electron affinity (EA) and ionization potential (IP), locally distributed by the Fukui functions.[47]

The definition proposed in eq 9 comes from chemical intuition, considering, for instance, that a hard electrophilic species would be one with a high IP, i.e., with very low tendency to donate electrons, possibly being positively charged and seeking other electron rich regions, driven by electrostatic interaction instead of electron density delocalization, which would be a soft type of interaction. This local hardness formulation is very dependent on the Fukui functions which, by definition, describe orbital controlled interactions and are significantly more related to local softness.

$$H_K^D = \mathrm{IP} f^-(r) - \mathrm{EA} f^+(r) \tag{9}$$

Hardness Pair Interaction. In this study, we will define ways to estimate these interactions between a pair of atoms: the atom that will be transferred and the atom with which the first one will form a bond. The charge transfer between the reactive atoms, estimated using the RDs, already was defined and tested for common organic reactions by Korchowiec and co-workers,[48] applying the Fukui functions calculated with finite differences. In this study, we focused on the hard−hard interaction through our extended RD for the atom pair defining the hardness pair interaction (HPI) RD.

For a pair of atoms the charge transfer pair (CTP) is the product of EAS of α atom and the NAS of β atom divided by their Euclidean distance $R_{\alpha\beta}$, as in eq 10. Here, α is defined as the atom with higher EAS in the pair. Inspired in this definition, HPI is defined in the same way, for each σ local hardness method, as shown in eq 11. HPIs were calculated for the reaction coordinate trajectory in the QC/MM calculations of the three enzymatic reactions treated in the present study.

$$\mathrm{CTP}_{\alpha\beta} = \frac{f_\alpha^- f_\beta^+}{R_{\alpha\beta}} \tag{10}$$

$$\mathrm{HPI}_{\alpha\beta}^{\sigma} = \frac{H_\alpha^\sigma H_\beta^\sigma}{R_{\alpha\beta}} \tag{11}$$

RESULTS AND DISCUSSIONS

Triosephosphate Isomerase. We have shown and analyzed the RDs results for the simulated reaction coordinate for the first catalytic cycle of TIM. In Figure 3, we show the variation in the heat of formation for the extraction of H1 from DHAP by GLU165. With the exception of PM6, all the other Hamiltonians resulted in an energy barrier of about 15 kcal/mol for the proton transfer, and AM1 achieved the most accurate intermediate state, showing that the first step is endothermic. These results are in agreement with computational simulation studies using DFT methods in QM/MM protocols, for a QC region of 200 atoms,[33] a semiempirical region of 450,[49] and with the experimental energy barrier of 13 kcal/mol.[50]

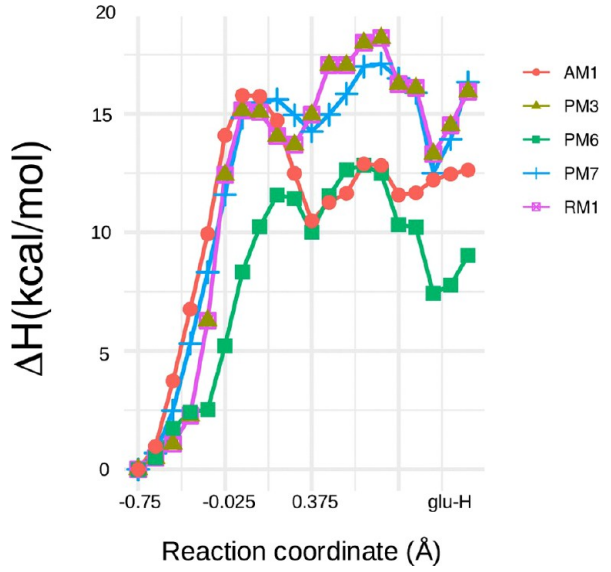

Figure 3. Variation of the enthalpy of formation for the simulated reaction coordinate geometries of the TIM catalysis first elementary step, the GLU165 residue protonation (glu-H) through the H1 extraction from DHAP.

We show in Figure 4 the results of HPI over the reaction coordinate, which estimates the hard−hard interactions between the proton that will be transferred and the glutamic oxygen that will receive it. The HPI calculated with local hardness method A, based on electron−electron potential, as well as with the method C, based on local chemical potential approximation, showed the best reaction profile, reaching the maximum value at the frame corresponding to the intermediate state. Method B, based on the Fukui potential, also indicates an overall increase of the hard−hard interaction throughout the reaction but with no specific pattern and different behavior for each Hamiltonian applied. Method D, based on the local distribution of ionization potential and electron affinity, did not show any pattern.

The inability of the local hardness methods highly dependent on the Fukui function to describe this proton transfer may be caused by the electrostatic interactions controlling the process, such that methods which account for the electron density are expected to be more successful. As expected for a proton transfer, the local hardness can provide very reasonable reaction profiles, generally obeying the maximum hardness principle, which states that chemical systems at their maximum hardness are in their most stable state.[51]

Some relevant patterns can also be observed from the Fukui functions, as seen in the RD values for the reactive atoms shown in Figure 5. There is, for instance, abrupt variation in the EAS of the GLU165 oxygen atom near the frame corresponding to a transition state, which causes it to lose propensity to donate electron density. There is also the steep increase in the propensity of receiving electron density shown by the H1 atom of DHAP, reaching the NAS maximum value at the transition state frame and decreasing sharply to nearly zero.

In Figure 6 we show a ball-and-stick representation of the TIM QC atoms along with the catalytic residues (GLU165 and HIS96) and the substrate atoms. For the QC system we color each atom in accordance to the RD values, that were calculated

https://dx.doi.org/10.1021/acs.jcim.9b00860
J. Chem. Inf. Model. 2020, 60, 578−591

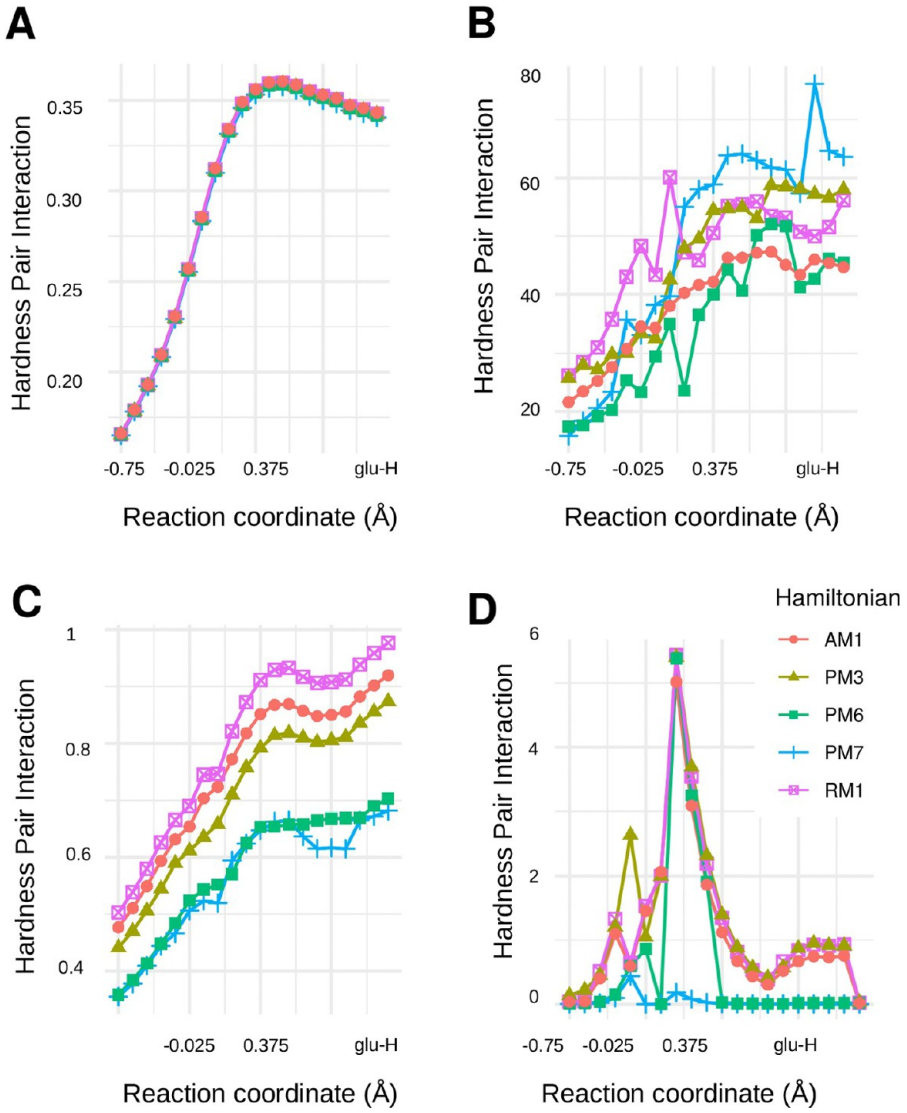

Figure 4. Hardness pair interaction from each local hardness method calculated for the OE2 atom of GLU165 and the H1 of GPA: A) H_K^A, B) H_K^B, C) H_K^C, and D) H_K^D.

from the electronic structure obtained with AM1, that showed the best energy profile for this reaction coordinate. We can observe that the highest values of local hardness concentrate mainly at the substrate atoms in the initial frame, showing the OE2 atom of GLU165 with higher local hardness than the OE1. This difference between the glutamic oxygens increases in the transition state frame and decreases in the last reaction coordinate. The transferred proton and the HIS96 proton hold the maximum local hardness values in the active site throughout the scan, which is interesting because these protons will be transferred in the following reaction step of TIM catalytic cycle.

Taking the difference of NAS and EAS we can estimate the net propensity of an atom acting as a Lewis base or acid, which is also known as the dual descriptor or dual Fukui function.[52] Using this RD, we show in Figure 6 the change in electron delocalization tendencies between the initial structure in the scan and its last one. The carboxyl oxygens show the lowest value of the dual descriptor, which means both a high propensity to donate electron density and to receive a proton. In the last simulated frame, the DHAP carbonyl oxygen is one of the most nucleophilic atoms, which means that it is apt to lose a proton. This is in agreement with the next step of the catalytic cycle, which is a proton transfer from HIS96 to DHAP.

Haloalkane Dehalogenase. Simulating the reaction coordinate of chlorine dissociation from dichloroethane (DCE) in the inverse way, we show in Figure 7 that the change in heat of formation during the relaxed scans with PM7 has to overcome an energy barrier of about 24 kcal/mol and has a reaction enthalpy of about 10 kcal/mol. The simulation displays the best similarity with other computational studies that used semiempirical methods,[21,53] which compared their results with experimental rate constants from the Kennes and co-workers study.[54]

Using these electronic structures from the trajectory, we calculated the HPI descriptor for the chlorine atom and the C2 of DCE, which are atoms that will make a bond along the reaction coordinate. We present in Figure 8 the HPI profiles using every local hardness method considered in this study. Methods A, B, and C show similar behavior among all semiempirical methods, indicating the increase in hard−hard

https://dx.doi.org/10.1021/acs.jcim.9b00860
J. Chem. Inf. Model. 2020, 60, 578−591

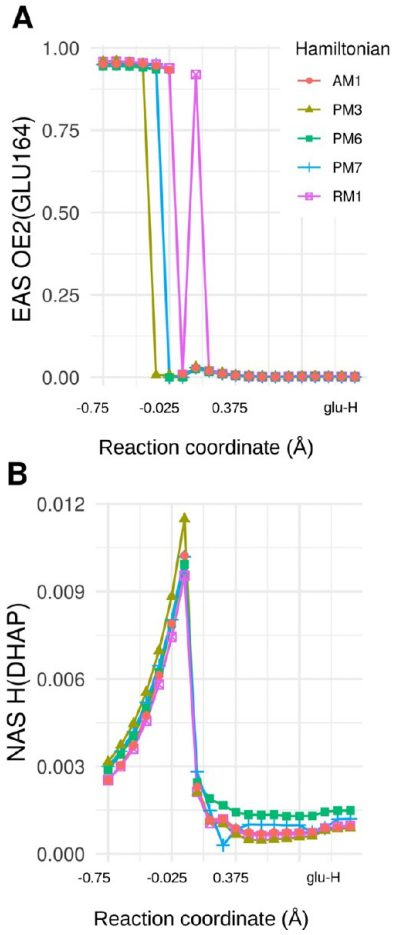

Figure 5. Reactivity descriptors calculated for the OE2 atom of GLU165 and the H1 of GPA from the AM1 electronic structure: A) electrophilic attack susceptibility for the OE2 (GLU165) and B) nucleophilic attack susceptibility for the H1 from DHAP.

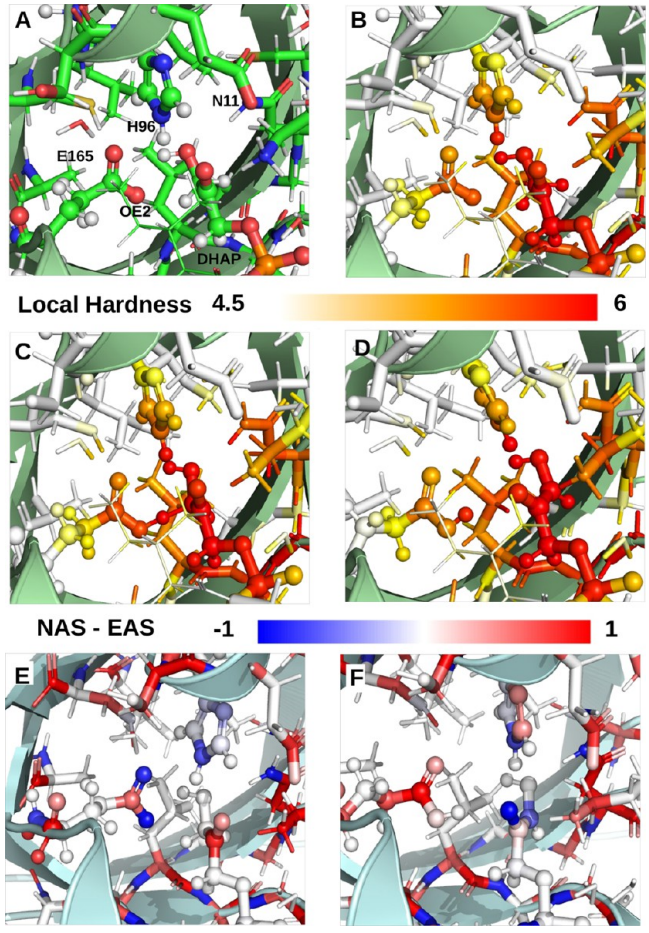

Figure 6. Reactivity descriptors calculated with the AM1 Hamiltonian for key simulated structures along the triosephosphate isomerase reaction coordinate of the first step in its catalytic cycle: A) TIM active site with atoms considered by quantum chemistry methods as a stick representation, the catalytic residues and substrate with their atom in ball representation as well, B) local hardness for the first reaction coordinate frame calculated with method A, C) local hardness for the fifth frame, D) local hardness for frame 19, E) difference between NAS and EAS for the first frame, and F) difference between NAS and EAS for the last frame.

interactions along the reaction coordinate, with methods A and B reaching the maximum value of HPI at the 20th and around the 15th scan frame, respectively.

The variation of local hardness for these atoms, calculated with method A shown in Figure 9, displays another pattern. The maximum value is reached for chlorine in the 11th frame, holding this value until the 15th frame. The DCE C2 atom local hardness reaches a maximum in the same structure as the chlorine atom, but the value starts to drop in the very next frame until bond formation.

In Figure 10a we depict HDH catalytic residues and the substrate, where the DCE is bound to ASP124 through its C1 carbon. Local hardness values for each atom are shown as well in Figure 10b for the initial structure, in Figure 10c for the determined TS, and in Figure 10d for the product of this reaction coordinate. These hardness values were obtained from the electronic structure of these geometries calculated with the RM1 Hamiltonian, that showed satisfactory energetic performance and provided the known nucleophilic behavior of chlorine ion. The DCE C2 atom appears as the hardest atom in the system, followed by the chlorine and the hydrogen atoms of TRP125 and GLU56 side chains, respectively, which are known to be the catalytic residues that stabilize the free chlorine. The hydrogen atoms of the pyrrolidine group in the TRP175 side chain also have high values of local hardness and are oriented toward the chlorine atom.

Adenosine Kinase. We show here the RD results for the third enzymatic catalysis simulated here, the transfer of a phosphoryl group from ATP to adenosine by the AK, yielding one adenosine monophosphate (AMP). In Figure 11 the potential energy surface is shown for the calculated atom transfers, using the heat of formation variation from the PM7 method, with a saddle point indicating an energy barrier of 10.22 kcal/mol and a heat of reaction of −8.86 kcal/mol.

In Figure 12 we show the key structures in the potential energy surface for these reaction coordinates. Figure 12a shows the initial structure for the scans, with the gamma phosphate at 3.2 Å from the oxygen-3 atom of the adenosine's ribose sugar and the proton bound to this oxygen at 1.9 Å from the oxygen OE2 of ASP31. A magnesium divalent cation and ARG129 are shown near to the gamma phosphate group of ATP, at 2.2 and 2.1 Å, respectively, for the closest hydrogen of ARG129 in relation to the nearest phosphate oxygen atom. After a displacement of 1.7 Å from the ATP, the phosphoryl assumes a trigonal planar conformation, slightly asymmetrical with two O−P−O angles of 124.4° and one of 111.2°, which is the

https://dx.doi.org/10.1021/acs.jcim.9b00860
J. Chem. Inf. Model. 2020, 60, 578−591

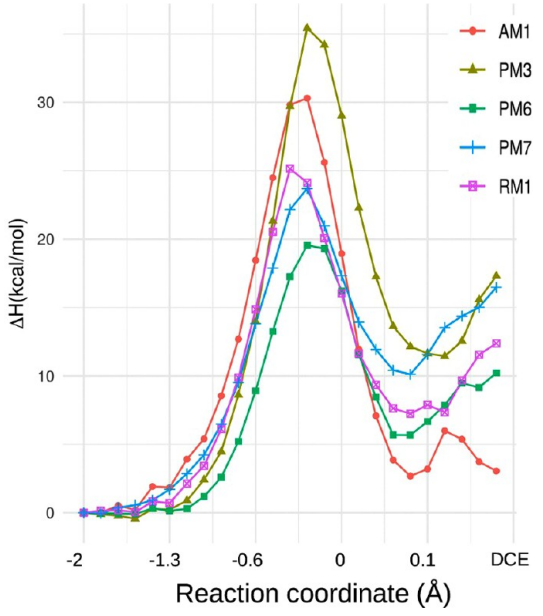

Figure 7. Variation in the enthalpy of formation for each frame along the reaction coordinate of the first step of the HDH catalytic cycle.

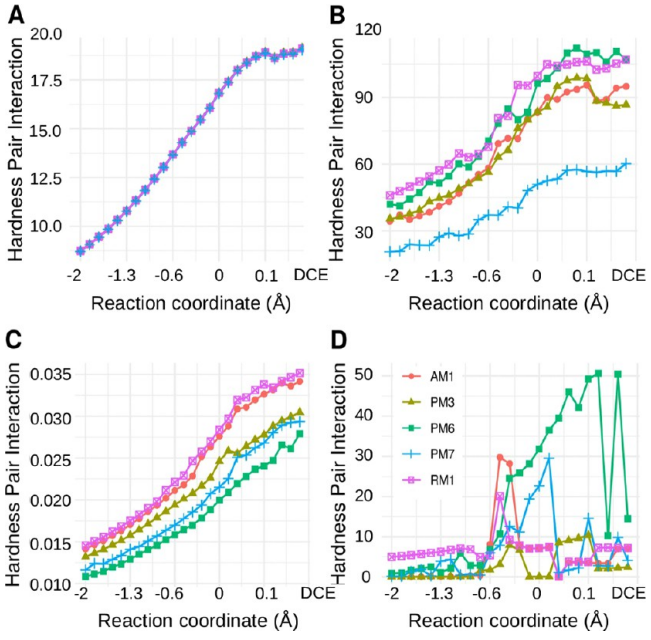

Figure 8. Hardness pair interaction for the four local hardness methods for each frame of HDH catlaysis: A) H_K^A, B)H_K^B, C) H_K^C, and D) H_K^D.

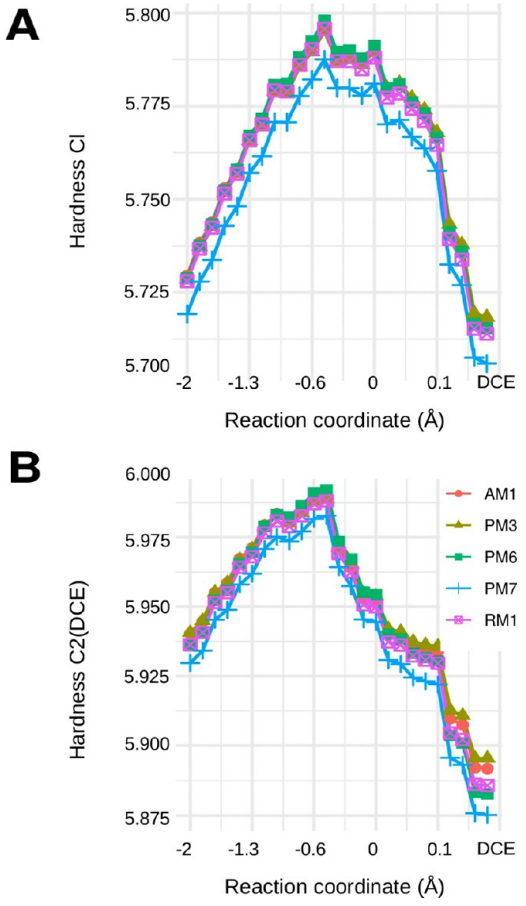

Figure 9. Local hardness of DCE relevant atoms obtained using method A for each frame of HDH catalysis: A) local hardness using the chlorine atom and B) local hardness for the C2 from dichloroethane.

closest to the Mg^{2+}. In this second structure (Figure 12b), the proton only distanced itself about 0.4 Å from the OE2 of ASP31. Figure 12c shows the final structure scan, the reaction products, that corresponds to the potential well that comes after the saddle point shown in Figure 11.

Through simulated thermodynamic information (variation of the heat of formation) and structural analysis we can estimate that the transfer of the phosphoryl occurs before the complete transfer of the adenosine proton to the ASP31 residue and that the arginine and Mg^{2+} must play an important role in the stabilization of the pentavalent phosphoryl trigonal planar group in the transition state of this reaction. Such a mechanism of reaction is already proposed by other active site structural studies.[23] Through the RD analysis of this reaction trajectory obtained from the PM7 scan, we explored the electronic structure information to depict what drives this reaction, the roles, and interactions within the QC region.

In Figure 13 we show the calculated HPI for the phosphoryl-accepting oxygen, as well as for its phosphorus, in a two-dimensional scan structure. For methods A, B, and C, which estimate HPI from local hardness, the maximum hard−hard interactions correspond to the formation of the most stable structures. For methods A and B, the hard−hard interactions between the gamma phosphorus and the adenosine oxygen increase more in the proton transfer coordinate direction, although this increase is sharper when the phosphoryl group has already been transferred, which is indicated by the potential energy surface obtained in this study. This can be interpreted as the proton transfer increasing the hard−hard nature of the phosphoryl transfer and giving more stability for the product.

In Figure 14 we show the local hardness of the active site atoms, calculated using method B, based on the Fukui potential, for some of the two-dimensional scan key structures. In all the structures shown in the picture, the ARG129 guanidino atoms and the Mg^{2+} close to the phosphoryl group presented the highest values of local hardness in the entirety of active site. This means that the RD applied here shows the strong electrostatic interactions of these atoms, which are very

https://dx.doi.org/10.1021/acs.jcim.9b00860
J. Chem. Inf. Model. 2020, 60, 578−591

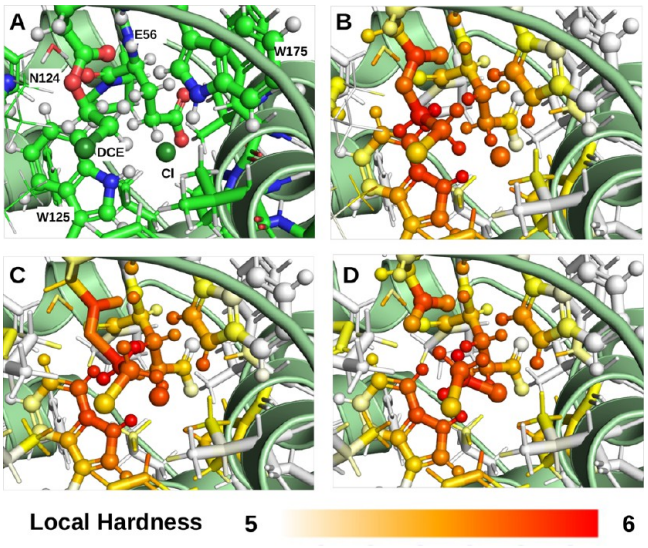

Figure 10. Reactivity descriptors calculated with the RM1 Hamiltonian for key structures along the coordinate of the haloalkane dehalogenase catalytic first step: A) HDH active site with atoms considered by quantum chemistry methods as stick representation, the catalytic residues and substrate with their atoms in ball representation as well, B) local hardness for the first reaction coordinate frame calculated with method A, C) local hardness for the fifth frame, and D) local hardness for frame 19.

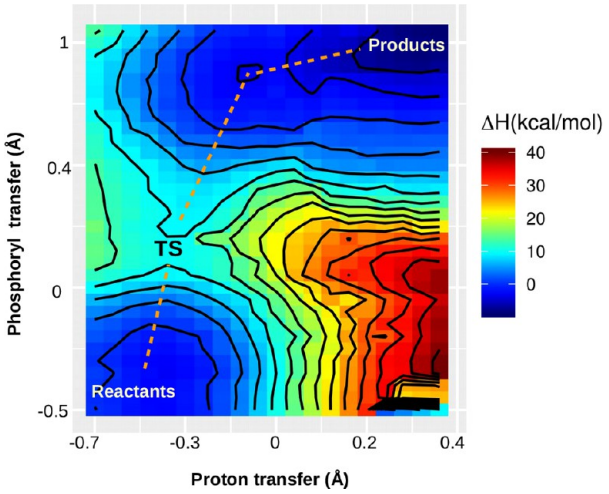

Figure 11. Contour plot of the heat of formation variation for the two-dimensional PM7 relaxed scans.

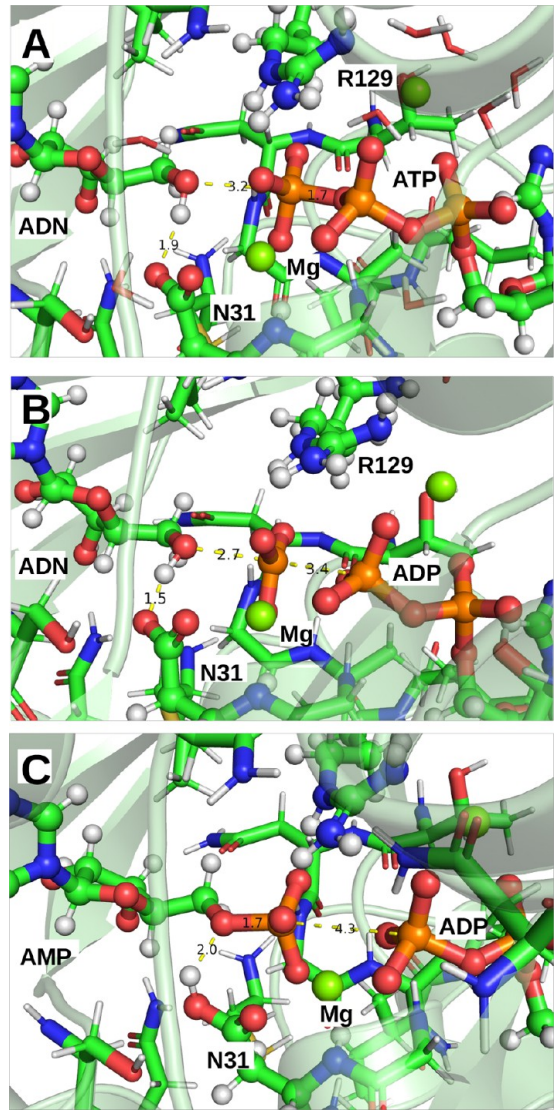

Figure 12. Key structures in the phosphoryl transfer from ATP to adenosine catalyzed by adenosine kinase obtained with a two-dimensional relaxed scan using the PM7 method. The substrates and catalytic amino-acid residues are shown in a ball-and-stick representation; the other atoms considered in the QC region are only in a stick representation: A) initial structure considered for the scan, B) structure corresponding to the heat of formation saddle point, and C) structure after the complete transfer of the phosphoryl group and the adenosine proton.

close to the transferred atoms in this reaction. Another relevant effect visualized here is that the Mg^{2+} cation near the gamma phosphate is slightly harder than the other one, which is near the alpha and beta phosphates of ATP molecule.

Figure 15 shows the dual Fukui function for the same structures shown in Figure 14, to enable the visualization of the major changes in the reactivity propensity of each atom during the reaction. In the first image (Figure 15a) we observe that all oxygen atoms of phosphate groups have the most negative values, something entirely expected based on the fact that ATP atoms concentrate negative charges. The adenosine ribose sugar that will bind to the gamma phosphorus shows dual values only greater than the phosphate oxygen atoms, indicating the propensity of receiving an electrophilic attack, and the gamma phosphorus shows a slightly positive value. The OE2 from ASP31, in this initial geometry, shows a near zero dual Fukui value, indicating that the propensity to donate charge in order to remove the adenosine proton is weak in the beginning of catalysis.

The cation Mg^{2+} shows one of the highest values for the dual Fukui RD, indicating its propensity to receive electron density, and the guanidino in ARG129 carbon shows the maximum value observed for this RD. In Figure 15b, we show our proposed TS for this mechanism in which the Mg^{2+} dual value increases, displaying a value significantly higher than the other Mg^{2+} that are far from the transferred atoms, in contrast to the ARG129 atom RD values that do not show changes. Another significant change in this second structure is in the phosphoryl atoms, of which the phosphorus increases its electrophilicity and the oxygen atom near the Mg^{2+} and ARG129 (O2G)

https://dx.doi.org/10.1021/acs.jcim.9b00860
J. Chem. Inf. Model. 2020, 60, 578−591

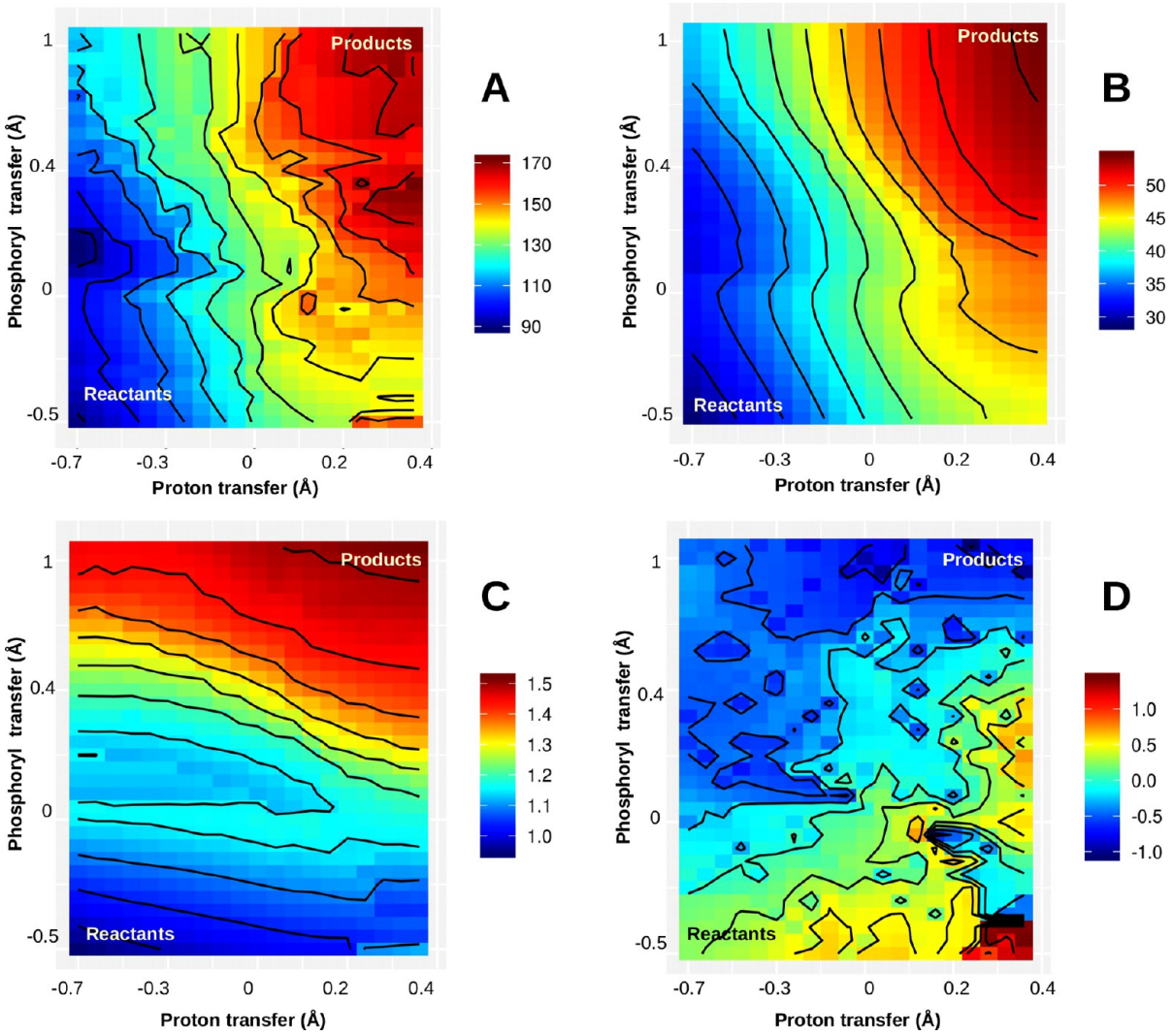

Figure 13. Hardness pair interaction between the adenosine ribose oxygen-3 and gamma phosphorus of ATP, calculated for structures taken from the simulated phosphoryl transfer and computed with a PM7 two-dimensional relaxed scan: A) H_K^A, B) H_K^B, C) H_K^C, and D) H_K^D.

concentrates the most negative values of dual Fukui, while the other two oxygens from the phosphoryl group show a decrease in their nucleophilicity. The RD is indicating here that the electron density in the phosphoryl group delocalizes and concentrates near the cation and ARG129 to be stabilized. Also, the adenosine oxygen involved in the reaction increases its nucleophilicity with the phosphoryl proximity.

In Figure 15c we show the dual Fukui RD for a structure with the adenosine monophosphate (AMP) already formed but with the proton transfer not completed (a displacement of only 0.4 Å in the ASP31 direction). The electronic structure information for this system shows that there is a significant increase in the nucleophilicity of the ASP31 oxygen atoms. We can also see that the phosphorus atom, which is in the AMP here, is significantly more electrophilic than the beta phosphate of the adenosine diphosphate (ADP).

The RD indicates two interesting things, the first is that the removal of the adenosine proton by ASP31 is facilitated by the transfer of the phosphoryl group, not the other way around, and the second is that the proton transfer is important to avoid the reaction reversion and ensure the product stabilization. Comparing the third and last structures shown in Figure 15, that presents the reaction product and the protonated ASP31, we can observe that the dual Fukui values for Mg^{2+} decrease to the same level of the other cation near the ADP phosphates, showing that the interaction roles of the two may be similar.

In Figure 16 we show the EAS values for the OE2 of ASP31 for each structure of the two-dimensional scan. It increases in the direction of the phosphoryl transfer reaction coordinate and decreases abruptly after a midway displacement in the proton transfer reaction coordinate, corroborating with the stepwise mechanism hypothesis. The RDs also confirm the role of ARG129 and Mg^{2+} cation, which were thought to be crucial for catalysis according to experimental studies.[55] We did not found any record of QC/MM simulations of these reaction coordinates, although a similar system was treated by McClory and co-workers,[56] the catalysis of mavalonate-5-phosphate by the mavalonate kinase. The reaction that occurs holds significant resemblance with AKs and involves the transfer of a phosphoryl group from an ATP molecule to the mavalonate, with a Mg^{2+} cation as a cofactor and a charged arginine and lysine amino-acid residue stabilizing the phosphoryl group in the TS geometry, which also holds remarkable similarities with AKs' TS.

Additionally, notice how the application of the correct CDFT RDs allows for the phenomenon to be described in

https://dx.doi.org/10.1021/acs.jcim.9b00860
J. Chem. Inf. Model. 2020, 60, 578−591

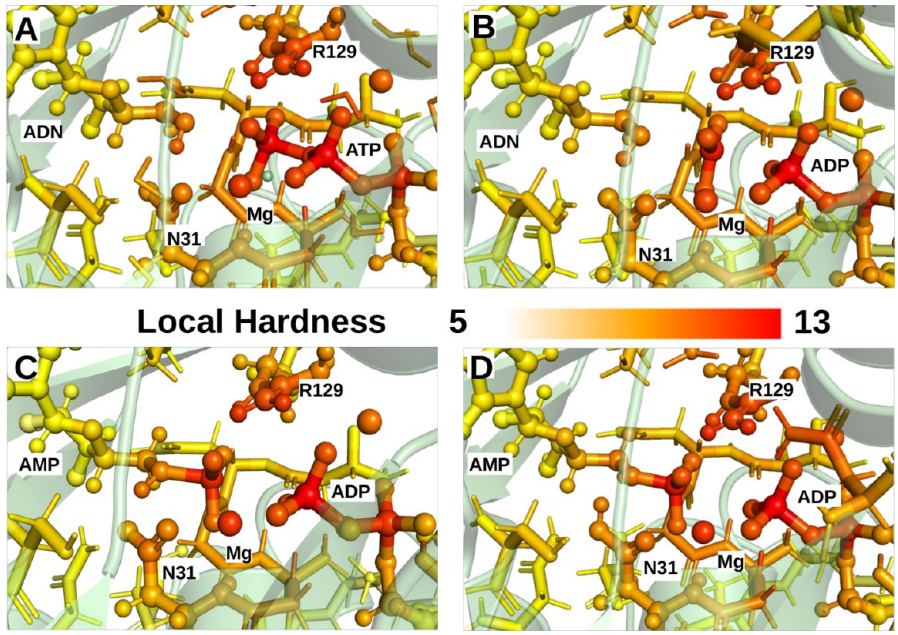

Figure 14. Local hardness, using method B, for the adenosine kinase active site for key structures of the two-dimensional simulated reaction scan: A) initial structure considered for the scan, B) structure corresponding to the heat of formation saddle point, C) structure after the complete transfer of the phosphoryl group, and D) structure after the complete transfer of the phosphoryl group and the adenosine proton.

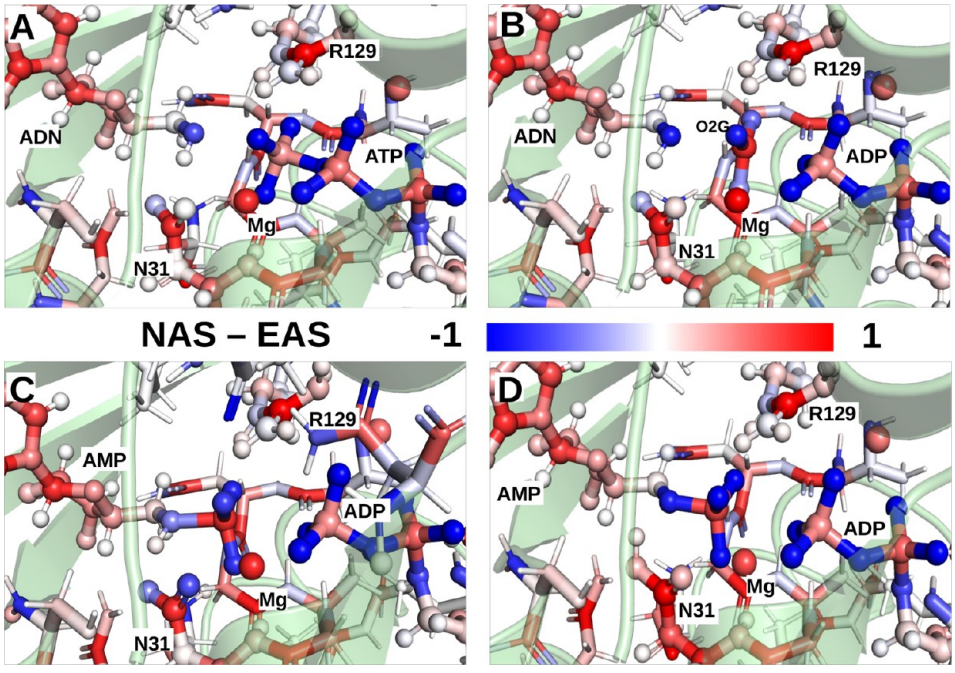

Figure 15. Dual Fukui function, the difference between electrophilic and nucleophilic attack susceptibilities, for the adenosine kinase active site for key structures in the two-dimensional reaction scan using the PM7 electronic structure method: A) initial structure considered for the scan, B) structure corresponding to the heat of formation saddle point, C) structure after the complete transfer of the phosphoryl group, and D) structure after the complete transfer of the phosphoryl group and the adenosine proton.

accordance with high-level quantum chemistry computations but in terms of well-known chemical terms and interaction types. This, together with all data presented until this point, shows how the electronic structure monitoring can be used to confirm or conjecture mechanism paths based on the atoms reactivity propensity and how the proper utilization of CDFT poses an interesting framework for the rigorous definition of chemical terms, enriching the analysis without compromising clarity.

We observed in the studied enzymatic catalysis that the local hardness of the atoms in the active site does not change substantially, even more so for the amino-acid residues that are said to stabilize the reaction structures. This corroborates with the theory that the lowering of the activation energy caused by enzymes is due to the electrostatic environment of the active sites, being appropriate for the transition state structure stabilization.[42] The other theory that can be considered is that the complex formation between the substrates and enzyme

https://dx.doi.org/10.1021/acs.jcim.9b00860
J. Chem. Inf. Model. 2020, 60, 578−591

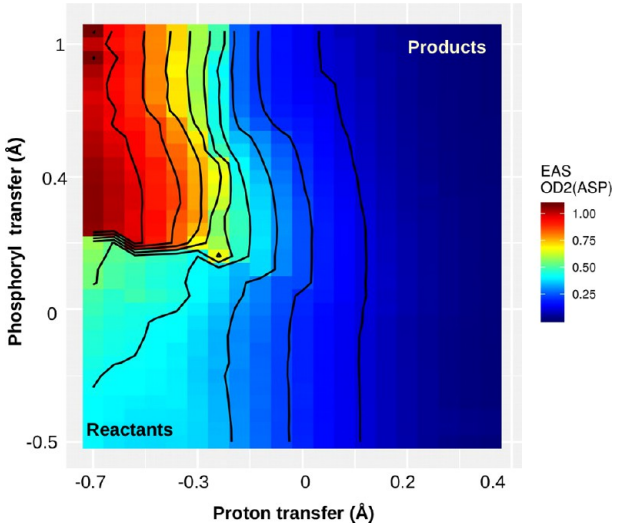

Figure 16. Electrophilic attack susceptibility for the carboxyl oxygen atom in the ASP31 acid residue that extracts the proton from the adenosine for all structures of the two-dimensional scan simulated with PM7.

causes conformation changes that are sufficient to progress to a TS with lower energy, thus lowering the activation barrier.[1] Although, for the calculated RDs depicting the "philicities", we observed abrupt changes along the reaction coordinates, showing the active participation of the enzyme in the transfer of atoms.

The capacity of the proposed atom pair RD based on hard−hard interactions to correctly outline a reaction profile is very dependent on the local hardness calculation method. For electron−electron potential based local hardness, method A, the HPI increases along the reaction coordinate, reaching its maximum value after a stable intermediary structure is formed. This behavior was repeated for method B, based on the Fukui potential, in the HDH and AK cases, and for method C, based on the local chemical potential approximation, in the TIM catalysis simulation. Method D, based on the distribution of IP and EA values pondered by the Fukui functions, did not show any pattern that could be used to study enzymatic reaction mechanisms.

What we can draw from the application of RDs is that it is possible to combine the accounting of electrostatic interactions and the electron density flow propensity of all involved atoms, perceiving the enzymatic effect of enhancing reaction rates rising from its intrinsic chemical reactivity as well, which can be retrieved from their electronic structure using low level computational chemistry methods.

CONCLUSIONS

In this study we apply theoretical quantities, that are well established for organic common reactions, to rationalize enzymatic catalysis, employing and discussing the appropriate modifications needed to deal with the electronic structure of large systems. Also, an atom pair interaction descriptor was proposed for monitoring the electrostatic interactions between the main atoms in the reactions, showing the working equations that can be useful in finding key structures in the reaction coordinates.

For the three enzymatic reactions studied here, the adenosine kinase catalysis mechanism first step was reported, for the first time, using two-dimensional reaction coordinates relaxed scans. From the PM7 potential energy surface results we provide a reasonable estimate of the reaction barrier, transition state structure, and reaction paths showing that the transfer of the phosphoryl atom to the adenosine occurs first, followed by the adenosine proton removal by the enzyme. The reactivity descriptors indicate the roles of the Mg^{2+} cation and catalytic residues present in the AK active site, the reaction propensities of the substrate molecules, and the right order of the transfers.

We expect that electronic structure monitoring of enzymatic catalysis will be useful to propose/predict/confirm new mechanisms and provide the description of roles for each amino-acid residue within a quantitative scale of chemical concepts, therefore, hastening the process of transforming the resolved protein three-dimensional structures into their equivalent catalytic information.

ASSOCIATED CONTENT

Supporting Information

The Supporting Information is available free of charge at https://pubs.acs.org/doi/10.1021/acs.jcim.9b00860.

Calculated absolute heat of formation for each stationary point simulated from relaxed scans, Tables S1−S3 (PDF)

AUTHOR INFORMATION

Corresponding Author

Gerd Bruno Rocha − *Federal University of Paraíba, João Pessoa, Brazil;* orcid.org/0000-0001-9805-9497; Phone: +55-83-3216-7437; Email: gbr@quimica.ufpb.br; Fax: +55-83-3216-7437

Other Authors

Igor Barden Grillo − *Federal University of Paraíba, João Pessoa, Brazil*

Gabriel A. Urquiza-Carvalho − *Federal University of Pernambuco, Recife, Brazil*

José Fernando Ruggiero Bachega − *Federal University of Health Sciences of Porto Alegre, Porto Alegre, Brazil*

Complete contact information is available at: https://pubs.acs.org/10.1021/acs.jcim.9b00860

Notes

The authors declare no competing financial interest.

ACKNOWLEDGMENTS

The authors gratefully acknowledge the financial support from following the Brazilian agencies, institutes, and networks: Instituto Nacional de Ciência e Tecnologia de Nanotecnologia para Marcadores Integrados (INCT-INAMI), Conselho Nacional de Desenvolvimento Científico e Tecnológico (CNPq), Coordenação de Aperfeiçoamento de Pessoal de Nível Superior - Brasil (CAPES), Programa de Apoio a Núcleos de Excelência (PRONEX-FACEPE), and Financiadora de Estudos e Projetos (FINEP). The authors also acknowledge the physical structure and computational support provided by the Universidade Federal da Paraíba (UFPB) and the computer resources of the Centro Nacional de Processamento de Alto Desempenho em São Paulo (CENAPAD-SP). This study was financed in part by the

Coordenação de Aperfeiçoamento de Pessoal de Nível Superior - Brasil (CAPES) through the research project Bioinformática Estrutural de Proteínas: Modelos, Algoritmos e Aplicações Biotecnológicas (Edital Biologia Computacional 51/2013, processo AUXPE1375/2014 da CAPES). G.B.R. acknowledges support from the Brazilian National Council for Scientific and Technological Development (CNPq grant no. 309761/2017-4).

REFERENCES

(1) Martí, S.; Roca, M.; Andrés, J.; Moliner, V.; Silla, E.; Tuñón, I.; Bertrán, J. Theoretical Insights in Enzyme Catalysis. *Chem. Soc. Rev.* **2004**, *33*, 98−107.
(2) Van Der Kamp, M. W.; Mulholland, A. J. Combined Quantum Mechanics/Molecular Mechanics (QM/MM) Methods in Computational Enzymology. *Biochemistry* **2013**, *52*, 2708−2728.
(3) Lonsdale, R.; Ranaghan, K. E.; Mulholland, A. J. Computational Enzymology. *Chem. Commun. (Cambridge, U. K.)* **2010**, *46*, 2354−2372.
(4) Martins, A. C.; Ribeiro, F. W.; Zanatta, G.; Freire, V. N.; Morais, S.; de Lima-Neto, P.; Correia, A. N. Modeling of Laccase Inhibition by Formetanate Pesticide using Theoretical Approaches. *Bioelectrochemistry* **2016**, *108*, 46−53.
(5) Melo, M. C. R. NAMD Goes Quantum: An Integrative Suite for QM/MM Simulations. *Nat. Methods* **2018**, *15*, 351.
(6) Mulholland, A. J. Modelling Enzyme Reaction Mechanisms, Specificity and Catalysis. *Drug Discovery Today* **2005**, *10*, 1393−1402.
(7) Raha, K.; Peters, M. B.; Wang, B.; Yu, N.; Wollacott, A. M.; Westerhoff, L. M.; Merz, K. M., Jr The Role of Quantum Mechanics in Structure-Based Drug Design. *Drug Discovery Today* **2007**, *12*, 725−731.
(8) Geerlings, P.; De Proft, F.; Langenaeker, W. Conceptual Density Functional Theory. *Chem. Rev.* **2003**, *103*, 1793−1874.
(9) Li, Y.; Evans, J. The Hard-Soft Acid-Base Principle in Enzymatic Catalysis: Dual Reactivity of Phosphoenolpyruvate. *Proc. Natl. Acad. Sci. U. S. A.* **1996**, *93*, 4612−4616.
(10) Roos, G.; Foloppe, N.; Van Laer, K.; Wyns, L.; Nilsson, L.; Geerlings, P.; Messens, J. How Thioredoxin Dissociates its Mixed Disulfide. *PLoS Comput. Biol.* **2009**, *5*, No. e1000461.
(11) Roos, G.; Loverix, S.; De Proft, F.; Wyns, L.; Geerlings, P. A Computational and Conceptual DFT Study of the Reactivity of Anionic Compounds: Implications for Enzymatic Catalysis. *J. Phys. Chem. A* **2003**, *107*, 6828−6836.
(12) Parr, R. G.; Yang, W. Density Functional Approach to the Frontier-Electron Theory of Chemical Reactivity. *J. Am. Chem. Soc.* **1984**, *106*, 4049−4050.
(13) Fukui, K. *Orientation and Stereoselection*; Springer: 1970; pp 1−85, DOI: 10.1007/BFb0051112.
(14) Pearson, R. G. Recent Advances in the Concept of Hard and Soft Acids and Bases. *J. Chem. Educ.* **1987**, *64*, 561.
(15) Domingo, L. R.; Ríos-Gutiérrez, M.; Pérez, P. Applications of the Conceptual Density Functional Theory Indices to Organic Chemistry Reactivity. *Molecules* **2016**, *21*, 748.
(16) Domingo, L. Molecular Electron Density Theory: a Modern View of Reactivity in Organic Chemistry. *Molecules* **2016**, *21*, 1319.
(17) Pearson, R. G. Absolute Electronegativity and Hardness: Applications to Organic Chemistry. *J. Org. Chem.* **1989**, *54*, 1423−1430.
(18) Roos, G.; Geerlings, P.; Messens, J. Enzymatic Catalysis: the Emerging Role of Conceptual Density Functional Theory. *J. Phys. Chem. B* **2009**, *113*, 13465−13475.
(19) Khandogin, J.; York, D. M. Quantum Descriptors for Biological Macromolecules from Linear-Scaling Electronic Structure Methods. *Proteins: Struct., Funct., Genet.* **2004**, *56*, 724−737.
(20) Fukushima, K.; Wada, M.; Sakurai, M. An Insight into the General Relationship Between the Three Dimensional Structures of Enzymes and Their Electronic Wave Functions: Implication for the Prediction of Functional Sites of Enzymes. *Proteins: Struct., Funct., Genet.* **2008**, *71*, 1940−1954.
(21) Kutỳ, M.; Damborskỳ, J.; Prokop, M.; Koca, J. A Molecular Modeling Study of the Catalytic Mechanism of Haloalkane Dehalogenase. Quantum Chemical Study of Complete Reaction Mechanism. *J. Chem. Inf. Model.* **1998**, *38*, 736−741.
(22) Richard, J. P. A Paradigm for Enzyme-Catalyzed Proton Transfer at Carbon: Triosephosphate Isomerase. *Biochemistry* **2012**, *51*, 2652−2661.
(23) Schumacher, M. A.; Scott, D. M.; Mathews, I. I.; Ealick, S. E.; Roos, D. S.; Ullman, B.; Brennan, R. G. Crystal Structures of Toxoplasma Gondii Adenosine Kinase Reveal a Novel Catalytic Mechanism and Prodrug Binding. *J. Mol. Biol.* **2000**, *296*, 549−567.
(24) Berman, H. M.; Bourne, P. E.; Westbrook, J.; Zardecki, C. *Prot. Struc.*; CRC Press: 2003; Chapter 14, pp 394−410.
(25) Wang, J.; Wolf, R. M.; Caldwell, J. W.; Kollman, P. A.; Case, D. A. Development and Testing of a General Amber Force Field. *J. Comput. Chem.* **2004**, *25*, 1157−1174.
(26) Field, M. J. The pDynamo Program for Molecular Simulations Using Hybrid Quantum Chemical and Molecular Mechanical Potentials. *J. Chem. Theory Comput.* **2008**, *4*, 1151−1161.
(27) Bachega, J. F. R.; Timmers, L. F. S.; Assirati, L.; Bachega, L. R.; Field, M. J.; Wymore, T. GTKDynamo: A PyMOL Plug-in for QC/MM Hybrid Potential Simulations. *J. Comput. Chem.* **2013**, *34*, 2190−2196.
(28) Dewar, M. J.; Zoebisch, E. G.; Healy, E. F.; Stewart, J. J. Development and Use of Quantum Mechanical Molecular Models. AM1: a New General Purpose Quantum Mechanical Molecular Model. *J. Am. Chem. Soc.* **1985**, *107*, 3902−3909.
(29) Rocha, G. B.; Freire, R. O.; Simas, A. M.; Stewart, J. J. P. RM1: A Reparameterization of AM1 for H, C, N, O, P, S, F, Cl, Br, and I. *J. Comput. Chem.* **2006**, *27*, 1101.
(30) Stewart, J. J. Optimization of Parameters for Semiempirical Methods. III Extension of PM3 to Be, Mg, Zn, Ga, Ge, As, Se, Cd, In, Sn, Sb, Te, Hg, Tl, Pb, and Bi. *J. Comput. Chem.* **1991**, *12*, 320−341.
(31) Saito, R.; Pruet, J. M.; Manzano, L. A.; Jasheway, K.; Monzingo, A. F.; Wiget, P. A.; Kamat, I.; Anslyn, E. V.; Robertus, J. D. Peptide-Conjugated Pterins as Inhibitors of Ricin Toxin A. *J. Med. Chem.* **2013**, *56*, 320−329.
(32) Stewart, J. J. Optimization of Parameters for Semiempirical Methods VI: More Modifications to the NDDO Approximations and Re-optimization of Parameters. *J. Mol. Model.* **2013**, *19*, 1−32.
(33) Guallar, V.; Jacobson, M.; McDermott, A.; Friesner, R. A. Computational Modeling of the Catalytic Reaction in Triosephosphate Isomerase. *J. Mol. Biol.* **2004**, *337*, 227−239.
(34) Harris, T. K.; Cole, R. N.; Comer, F. I.; Mildvan, A. S. Proton transfer in the mechanism of triosephosphate isomerase. *Biochemistry* **1998**, *37*, 16828−16838.
(35) Kowaluk, E. A.; Jarvis, M. F. Therapeutic Potential of Adenosine Kinase Inhibitors. *Expert Opin. Invest. Drugs* **2000**, *9*, 551−564.
(36) Andersson, C. E.; Mowbray, S. L. Activation of ribokinase by monovalent cations. *J. Mol. Biol.* **2002**, *315*, 409−419.
(37) Parr, R. G.; Pearson, R. G. Absolute Hardness: Companion Parameter to Absolute Electronegativity. *J. Am. Chem. Soc.* **1983**, *105*, 7512−7516.
(38) Yang, W.; Parr, R. G.; Pucci, R. Electron Density Kohn−Sham Frontier Orbitals and Fukui functions. *J. Chem. Phys.* **1984**, *81*, 2862−2863.
(39) Pearson, R. G. Recent Advances in the Concept of Hard and Soft Acids and Bases. *J. Chem. Educ.* **1987**, *64*, 561.
(40) Sánchez-Márquez, J.; Zorrilla, D.; García, V.; Fernández, M. Introducing a New Methodology for the Calculation of Local Philicity and Multiphilic Descriptor: an Alternative to the Finite Difference Approximation. *Mol. Phys.* **2018**, *116*, 1737−1748.
(41) Ribeiro, A. J. M.; Holliday, G. L.; Furnham, N.; Tyzack, J. D.; Ferris, K.; Thornton, J. M. Mechanism and Catalytic Site Atlas (M-CSA): a Database of Enzyme Reaction Mechanisms and Active Sites. *Nucleic Acids Res.* **2018**, *46*, D618−D623.

(42) Warshel, A.; Sharma, P. K.; Kato, M.; Xiang, Y.; Liu, H.; Olsson, M. H. Electrostatic Basis for Enzyme Catalysis. *Chem. Rev.* **2006**, *106*, 3210−3235.
(43) Chattaraj, P. K.; Roy, D. R.; Geerlings, P.; Torrent-Sucarrat, M. Local hardness: a Critical Account. *Theor. Chem. Acc.* **2007**, *118*, 923−930.
(44) Torrent-Sucarrat, M.; De Proft, F.; Ayers, P. W.; Geerlings, P. On the Applicability of Local Softness and Hardness. *Phys. Chem. Chem. Phys.* **2010**, *12*, 1072−1080.
(45) Cárdenas, C.; Tiznado, W.; Ayers, P. W.; Fuentealba, P. The Fukui Potential and the Capacity of Charge and the Global Hardness of Atoms. *J. Phys. Chem. A* **2011**, *115*, 2325−2331.
(46) Gal, T.; Geerlings, P.; De Proft, F.; Torrent-Sucarrat, M. A New Approach to Local Hardness. *Phys. Chem. Chem. Phys.* **2011**, *13*, 15003−15015.
(47) Meneses, L.; Tiznado, W.; Contreras, R.; Fuentealba, P. A Proposal for a New Local Hardness as Selectivity Index. *Chem. Phys. Lett.* **2004**, *383*, 181−187.
(48) Korchowiec, J.; Uchimaru, T. The Charge Transfer Fukui Function: Extension of the Finite-Difference Approach to Reactive Systems. *J. Phys. Chem. A* **1998**, *102*, 10167−10172.
(49) Cui, Q.; Karplus, M. Quantum Mechanic Molecular Mechanics Studies of Triosephosphate Isomerase-Catalyzed Reactions: Effect of Geometry and Tunneling on ProtonTransfer Rate Constants. *J. Am. Chem. Soc.* **2002**, *124*, 3093−3124.
(50) Albery, W. J.; Knowles, J. R. Free-Energy Profile for the Reaction Catalyzed by Triosephosphate Isomerase. *Biochemistry* **1976**, *15*, 5627−5631.
(51) Pal, S.; Vaval, N.; Roy, R. Principle of Maximum Hardness: An Accurate Ab Initio Study. *J. Phys. Chem.* **1993**, *97*, 4404−4406.
(52) Martínez-Araya, J. I. Why is the Dual Descriptor a More Accurate Local Reactivity Descriptor Than Fukui Functions? *J. Math. Chem.* **2015**, *53*, 451−465.
(53) Damborskỳ, J.; Kutỳ, M.; Němec, M.; Koca, J. A Molecular Modeling Study of the Catalytic Mechanism of Haloalkane Dehalogenase: Quantum Chemical Study of the First Reaction Step. *J. Chem. Info. Comput. Scienc.* **1997**, *37*, 562−568.
(54) Kennes, C.; Pries, F.; Krooshof, G. H.; Bokma, E.; Kingma, J.; Janssen, D. B. Replacement of Tryptophan Residues in Haloalkane Dehalogenase Reduces Halide Binding and Catalytic Activity. *Eur. J. Biochem.* **1995**, *228*, 403−407.
(55) Maj, M. C.; Singh, B.; Gupta, R. S. Pentavalent Ions Dependency is a Conserved Property of Adenosine Kinase from Diverse Sources: Identification of a Novel Motif Implicated in Phosphate and Magnesium Ion Binding and Substrate Inhibition. *Biochemistry* **2002**, *41*, 4059−4069.
(56) McClory, J.; Lin, J.-T.; Timson, D. J.; Zhang, J.; Huang, M. Catalytic Mechanism of Mevalonate Kinase Revisited, a QM/MM study. *Org. Biomol. Chem.* **2019**, *17*, 2423−2431.

https://dx.doi.org/10.1021/acs.jcim.9b00860
J. Chem. Inf. Model. 2020, 60, 578−591